FR8501503

Applied superconductivity conference
San Diego, CA (USA) 9-13 Sep 1984
CEA-CONF--7744

NbN TUNNEL JUNCTIONS

J.C. VILLEGIER, L.VIEUX-ROCHAZ, M. GONICHE, P. RENARD, M. VABRE

Commissariat à l'Energie Atomique LETI-IRDI
85 X 38041 GRENOBLE CEDEX FRANCE

Abstract

All-Niobium Nitride Josephson junctions have been prepared successfully using a new processing called SNOP : Selective Niobium (Nitride) Overlap Process. Such a process involves the "trilayer" deposition on the whole wafer before selective patterning of the electrodes by optically controlled Dry Reactive Ion Etching. Only two photomask levels are need to define an "overlap" or a "cross-type" junction with a good accuracy.

The properties of the Niobium Nitride films deposited by DC-Magnetron sputtering and the surface oxide growth are analysed. The most critical point to obtain high quality and high gap value junctions resides in the early stage of the NbN counterelectrode growth. Some possibilities to overcome such a handicap exist even if the fabrication needs substrate temperatures below 250°C.

Introduction

Recently, much progress has been made in fabricating Nb-aSi-Nb, NbN-aSi-Nb, Nb-Al-oxide-Nb and (Nb-NbN)-oxide-(NbN-Nb) junctions using new integration processes called SNAP (Selective Niobium Anodization Process)[1,2] and SNEP (Selective Niobium Etching Process[3,4]. Development of Josephson junctions with high Tc superconductors is important from the point of view of stable operating devices when smalll temperature fluctuations occur or for operation at temperature near 10 K where small closed cycle refrigerators are becoming available. Moreover, junctions can be biased or generate large gap voltages (and frequencies) which are important for SIS, Voltage-Standard, Superconducting lines and Logic circuit applications. Good quality NbN films (Tc = 16 K) have been prepared by several groups using DC or RF sputtering deposition methods[5,6,7,8]. NbN-Pb junctions have been proved to be of high quality[9,10] and all-NbN junctions are found to be the most promising all-refractory diodes which can be elaborated at 250°C and baked at 300°C without significant degradation of the oxide tunnel barrier[4].
However, all-NbN junctions often present a substantial level of subgap leakage current, a drastic reduction and broadening of the counterelectrode energy gap.

A novel All-refractory fabrication process

A novel process for fabricating refractory superconducting tunnel junctions called SNOP :
Selective Niobium (Nitride) Overlap Process has been successfully tested on (Nb-NbN)-oxide-(NbN-Nb) and (Nb-Al-oxide-Nb) tunnel junctions.

The fabrication procedure described on fig.1 begins with the deposition of the trilayer sandwich : (Nb_I- NbN_I)-oxide-NbN_{II} on the entire surface of a 5 cm diameter sapphire (or silicon) wafer. The films are DC-Magnetron sputtered while the oxide is generally in situ thermally grown. The substrate is not heated above 200°C during these consecutive depositions.

The patterning of the trilayer is performed by Reactive Ion Etching using SF_6/O_2 mixtures, fig.2.

Manuscript received Sept.10, 1984

(Alcatel GIR 200 system). This gas was found[11] to lead to a high etching rate for Niobium and NbN_2 films (130 nm/mn) with low RF powers (0.12-0.15 W/cm^{-2})

15 % of oxygen leads to approximately equal etching rates for Niobium, Niobium Nitride and Resist. This condition was used to obtain edges developing an approximate 40° slope from the vertical for good step coverage by the following layers. The angle is approximately transferred from the edge angle of the previously baked resist layer.

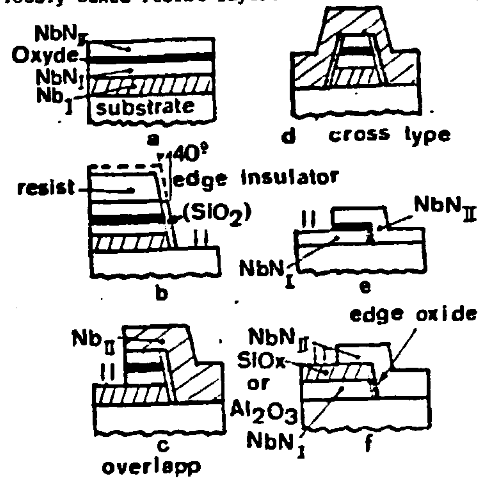

Figure 1 : Fabrication processes for a (Nb-NbN)/(NbN-Nb) (SNOP) junction : a, b, c, d, e, f : simpler processes for NbN/NbN overlap and edge junctions.

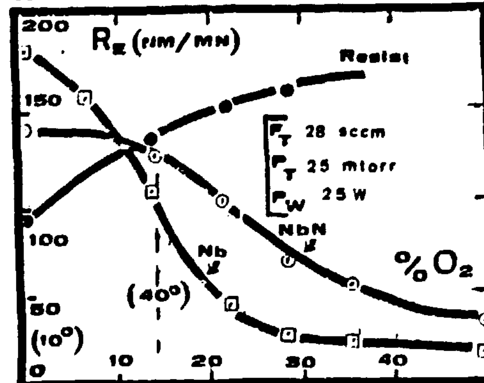

Figure 2 : RIE rates in a SF_6/O_2 mixture (Total flow 28 sccm, Power 25 W,P_{tot} 25 mtorr)
(I) First etching : (40°) (NbN_{II}/Ox/NbNI/NbI)
(II) Second etching : (10°) (Nb_{II}/NbN_I-Ox-NbN_I)

A thin (20 nm) insulating film is formed on the first electrode banks before removing the first resist mask (fig.1c). The process involves such an edge insulator to prevent subsequent shortening of the two electrodes. RF sputtered SiO_2, Al_2O_3 films or plasma oxides have been used for the insulating layer.

The upper Niobium contact film is deposited by DC (or RF) sputtering after a short backsputter cleaning of the NbN counterelectrode.

The patterning of the upper Nb contact is done (fig.1c) by Reactive Ion Etching in pure SF_6 gas with an optical control done by in-situ laser reflectometry. The process supposes the etching of Nb_{II}-NbN_{II}-Oxide-NbN_I consecutive films which has to be stopped at the NbN_I-Nb_I interface.
A large change of reflectance level is first observed when the Nb contact is removed, followed by weaker but easily detectable change at the oxide level at the Nb_I-NbN_I interface as shown on fig.3a with an accuracy better than 5 %.

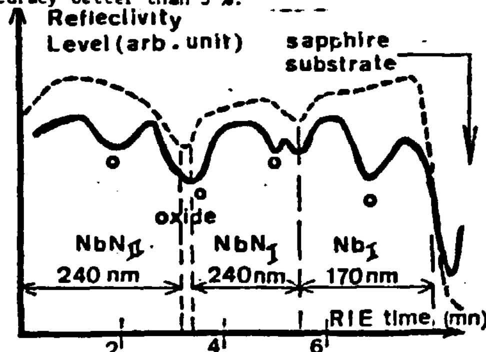

Figure 3 : Reflectivity profil during NbN_{II}-Ox-NbN_I-Nb RIE etching 15 % O_2/SF6 (a) without resist, (b) with resist stencil.

However, the reflectometry signal is generally affected by the interference inside the resist layer (fig.3b) ; to overcome such an artefact a test layer coming from the same deposition batch is generally etched before the patterned wafers, the interface identification is undoubted in this case. The use of the dry reactive ion etching technique permits to obtain an uniform etch better than 3 % on the whole wafer, and good dimension controlled junction area in the micrometer range as shown on fig.4 . The contacts on the NbN diodes are obtained by gold wire thermal bonding on AuGe pads.
The SNOP process involving only two mask levels, a whole wafer trilayer deposition and a dry controlled etching is well adapted for large scale and circuit integration. The most critical part is a good control of the edge an- gle and coverage by an adhesive insulating film. Plasma-oxidized films or 100 nm of sputtered dielectrics, especially SiO_2, (or Al_2O_3, TiO_2..) give a better insulator than evaporated SiOx which gives some cracks. Planarization could also in principle be done for instance with a spinon glass film deposited after the first etching step.
The SNOP process used for developing various sizes of overlap and cross-type junctions and arrays is found to give less parasitic areas, capacitances and more dense devices than comparative SNEP and SNAP diodes.

Simple overlap process :

Simple adaptation of the etching process is used in the study to define NbN-oxide-NbN overlap and edge junctions. The insulator of the edge junction is a 150 nm thick SiOx (or Al_2O_3) film deposited on the first electrode (fig.1f). The tunnel barrier is formed on the patterned first electrode by a light back sputter cleaning followed by a thermal xidation and counterelectrode deposition. The counterelectrode is patterned by SF_6/O_2 RIE with optically controlled end of attack. Such a process is well adapted to obtain small ($\approx 1\ \mu m^2$) diodes for DC-SQUIDs and SIS devices .

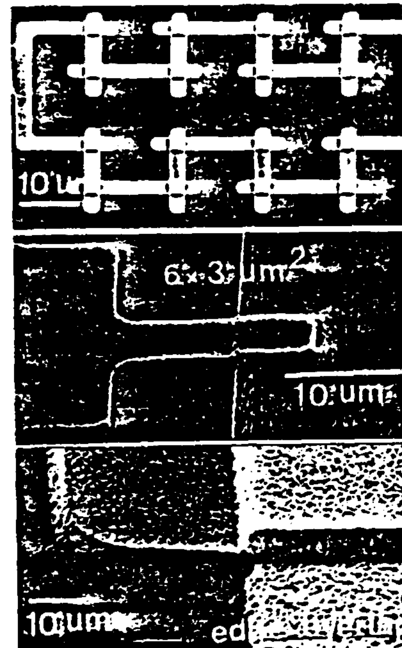

Figure 4 : SNOP (a) (b) and Overlap (c) junctions.

NbN film deposition properties

Film preparation

NbN thin films are deposited by DC-Magnetron Sputtering in Ar-N_2 mixtures with a commercial MRC 902 system. Background pressure is maintained below 2.10^{-7} torr by cryopumping and below 4.10^{-7} torr with the throttle valve partially opened before sputtering. Target is a MARZ grade pure Niobium, pure Nitrogen is used and Argon is purified in a Ti owen before introduction. High speed deposition rate is obtained (R_T = 200 nm by minute) for a lower density of about $14\ W.cm^{-2}$, on the simultaneous deposited (till 25) two inches, Silicon, Si + SiO_2, glass and sapphire wafers. Various Nb-N phases could be reached in increasing from zero the Nitrogen partial flow (F_{N2}/ F_{N2} + F_{Ar}) in the gas mixture as previously described . In this paper, only the single B1-BCC phase is studied in the experimental partial and total gas pressure range where the phase is obtained. It has been previously reported that stoechiometry, structural phase and film morphology depend on the preparation substrate temperature and pressure parameters.

The total pressure is found to be a critical factor governing the film growth, so three characteristic total pressures, respectively P_T = 10, 15 and 20 mtorr have been fixed. P_T and the flux ratio F_{N2}/ F_{Ar} are maintained constant during the process, the absolute Ar and N_2 gas flows are automatically feed-backed to the pressure and flow ratio set points. Substrates are either heated to obtain substrate temperatures in the range 100-300°C or not intentionally heated leading to a substrate self-heating temperature measured below 100°C.

Substrates are H-F sputter cleaned at low energy

before deposition and a presputtering procedure of about 10 minutes is necessary to stabilize the deposition parameters. The films prepared on silicon and sapphire substrates were characterized electrically in term of their temperature dependent resistivity $\rho(T)$ and precise sheet resistance measurements at 300 K
- Critical temperature is obtained with an absolute accuracy better than 0.2 K and transition width at 0.02 K, for standard measurements.

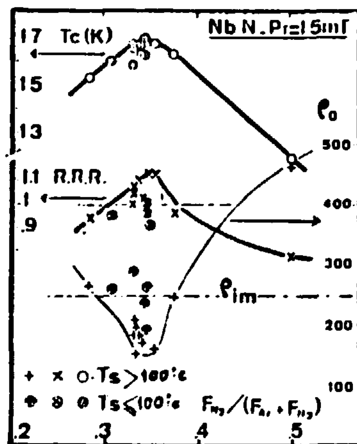

Figure 5 : Tc(K), ρ_{20K}, ρ_{300K}/ρ_{20K} versus Nitrogen flow (P_T = 15 mtorr)

High Tc films without heating

As pointed out by various authors[2, 10, 12] it is possible to reach Tc values above 15 K without substrate heating. However, the films show complex behaviors concerning the Tc, resistivity ratios and resistivity levels. It is found as shown on fig.5 that for a total pressure set at 15 mtorr the critical temperature can reach near 17 K for 400 nm thick films without substrate heating. Maxima for Tc(17 K), resistivity ratio ($\rho_{300K}/\rho_{20K} \simeq 1.15$) and minimum of resistivity ($\rho_{20K} \simeq 150\,\mu\Omega cm$) are found for the same Nitrogen partial flow value : $F_{N2}/(F_{N2} + F_{Ar}) = 0.34$. However, conductance levels for films deposited at room temperature are of the order of the maximum intragrain resistivity ($\rho_{im} \simeq 250\,\mu\Omega cm$) introduced by Hake[13].
Similar optimum Nitrogen flow values 0.29 and 0.48 are found for 10 mtorr and 20 mtorr of total gas pressures respectively (Table 1 and fig.6), maximum Tc being 14.8 K and 15.4 K without heating.
For each total pressure it exists a relation between Tc and resistive ratios with a maximum close to unity.

Low resistive ratios are found often related to high Nitrogen content in the film, while a sharp Tc decrease is found after the Tc max. leading to mixtures of B1-NbN with Niobium rich phases for large ρ_{300}/ρ_{20} values.

Table 1 : Dependence of film parameters on total pressure near the optimum Nitrogen flow $X = F_{N2}/(F_{N2} + F_{Ar}) \simeq Xo$.

P_T (mtorr)	Xo	Tc_M (K)	ρ_{20K} ($\mu\Omega cm$)	ρ_{300K}/ρ_{20}	$d\rho/dx$ mΩcm
10	0.29	15.	120	0.9	0.600
15	0.34	17.0	160	1.16	1.2
20	0.48	16.3	350	1.05	2.7

Film composition and crystalline structure

Nitrogen concentration and impurity levels are measured by RBS with 2 MeV $^4He^+$ ions and Nuclear Reactions on ^{14}N, ^{16}O, ^{12}C. Nitrogen content x in NbNx is found to increase from 0.9 to 1.5 with few variations of the lattice parameter of the single B1 phase when the Nitrogen flow is increased during sputtering for 15 or 20 mtorr total pressure.
Auber and Spitz[7] observed a similar variation associated with a large density decrease assuming that NbNx countains Niobium vacancies, maximum Tc corresponding to stoechiometry. However, as found by others, we observe for high Nitrogen content grain boundary enhancement and possible microvoids formation which can lead also to a density decrease. Levels of oxygen and carbon impurities are always found inferior to 1 at % in our films and nearly homogeneously repar- tited accross the film while some enhancement occurs near the upper film surface as verified by SIMS and Auger depth profils. For optimal gas flow values the main cristalline film properties are reported on fig.6 and table 1. for the three total pressure values :

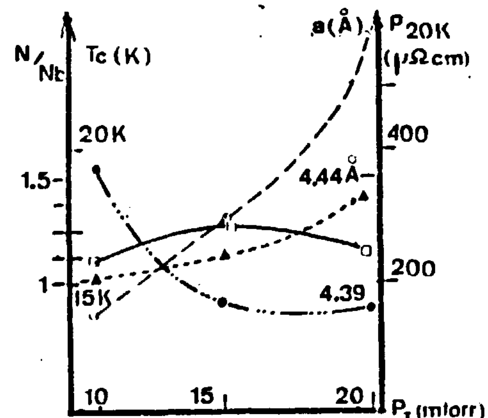

Figure 6 : Main parameters obtained for optimum N_2 gas flow versus P_T.

Low pressure depositions (P_T = 10 mtorr) show low resistivity levels ($\sim 120\,\mu\Omega$ cm) with a resistivity ratio close to unity. Films are found nearly in the stoechiometric composition however, the lattice parameter is strongly dilated a = 0.444 nm as found by Bacon et Al[8] (0.446 nm). The films are observed with small grain sizes ($\simeq$ 5 nm) and some light indication of two preferred orientations (200) and (111) perpendicular to the film surface. Compressive stresses developed in the films are found similar to those induced by Ar atoms bombarding the Niobium films during sputtering for the same low total pressure. Lattice dilatation is found to increase the Tc while the small grain size decreases the Tc values as observed on fig.7 where the low pressure data are about 1 K above the experimental curve. The resistivity of the film is probably in this case mainly due to local defects induced during the growth and to size effect mean free path limitations more than to grain boundary resistivity or impurity concentration.

Medium pressure (15 mtorr)

The films have a low stress level and a lattice parameter close to the 0.438 nm bulk value but contain some Nitrogen in excess ($N/Nb \simeq 1.1$) associated to the resistivity level increasing rapidly with Nitrogen flow.

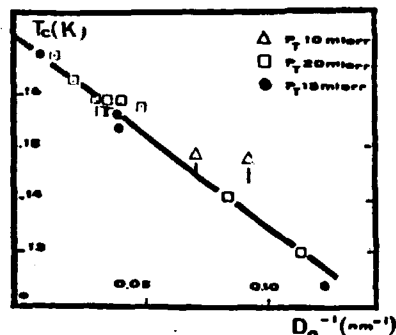

Figure 7 : Critical temperature versus grain size.

The grain size growths with the film thickness, between about 8 nm for a 40 nm thick film (Sample C) as shown on fig.8a, with random orientations to 20 x 50 nm for a 400 nm thick film showing a strong (111) preferred orientation. In these films resistivity is partially governed by grain boundary resistivity and partially by intragrain resistivity as shown on fig.6.

Large pressure (20 mtorr)

Films have high resistivity levels growing exponantially with Nitrogen concentration.

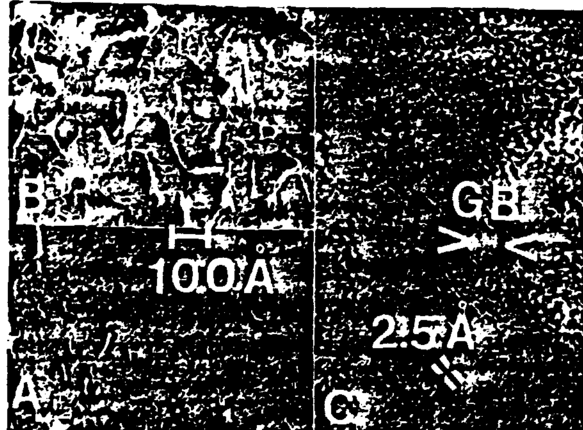

Figure 8 : Grain size observed by TEM :
a) Sample C : (40 nm thick, P_T = 15 mtorr)
b) Sample A : 82 nm thick, P_T = 20 mtorr with large grain boundary size

Films contain low stress levels but strong columnar (111) growth above 100 nm thick. As observed on fig.8b and c (Sample A), a 80 nm thick film had a nearly random orientation and grain size of about 12 nm diameter. Large amorphous grain boundaries surrounding the grains are directly observed by high resolution TEM. Vertical (111) crystalline planes are also seen on the picture with a 0.25 nm interplanar distance. Some mismatch and curvature are observed inside the diffracting grains indicating some intragrain defect formation during the sputtering. However, void formation is not clearly seen below 500 µΩcm resistivity. In these films, resistivity is principaly associated to resistive grain boundary formation.

Small grain size in the interfaces

The grain size is little dependent on the substrate temperature in the range 20°C-300°C indicating that the surface temperature and the NbN surface-plasma interaction govern the growth. When a double NbN-NbN film is done by two consecutive depositions without oxidation, the interface is clearly seen by SEM on a fracture and during etching with a change of reflectivity of about 15 %. A direct evidence of the small grain size near the oxide interface in a NbN-oxide-NbN junction is shown by TEM and SEM fracture on fig.9 where 5 nm size grains are separated by voids and an amorphous low density phase. Such an oxide-NbN_{II} interface leads to low Tc grains embedded in non superconductive material in the scale of coherence length which can explain the low gap value.

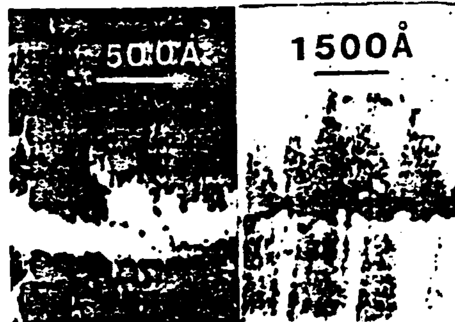

Figure 9 : Cross section of NbN-Oxide-NbN (A) TEM, (B) SEM.

Superconductive parameters

Resistivity and critical fields

DC-field measurements have been done in SNCI-Grenoble by O. Laborde up to 200 kOe on a thin granular film (sample A) 82 nm thick observed previously by TEM figure 8b, c deposited at 20 mtorr and on a 900 nm thick film deposited at 15 mtorr (sample B).

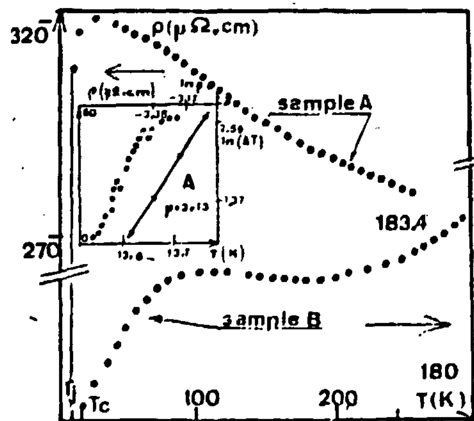

Figure 10 : Films resistive behavior.
Sample A (P = 20 mtorr)
Sample B (P = 15 mtorr)

The resistivity (T) observed on the two samples shows completely different behaviors (fig.10) :
Sample A fits well a Mott hopping conduction equation as observed by Jones[14] and Kampwith[6].
$\mathrm{LnG}(T) = \mathrm{Ln}\,G_0 - (T_0/T)^{1/4}$
with $G_0 = 225^{-1}\,(\mu\Omega cm)^{-1}$ and T_0 = 0.91 K associated with a smooth superconductive transition between T_J = 13.58 K onset of resisitivity corresponding to phase looking superconductivity and T_G which is defined as the maximum of the resistivity. T_G corresponds to the crossover between localisation effects and grain superconductivity.
T_G = 16.21 K and R_T follows a variation $R_T \sim (T_J - T)^{\mu}$, μ = 3.13 near T_J.

Sample B exhibits a complex "metallic" behavior with some maxima at about 110 K followed by a linear resistivity decrease below 80 K and a sharp superconductive transition at Tc = 16.43 K, Tc = 0.07 K. Such types of $\rho(T)$ behavior are reminiscent of those of high Tc_5 - W compounds and B1 - VNx observed by Zhao et Al[15] but probably masked by some excess grain boundary resistivity ($\simeq 100 \mu\Omega cm$).

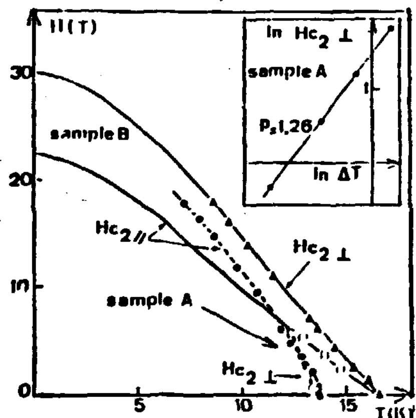

Figure 11 : Critical field data

Critical fields present also very different behaviors :

Sample A : Hc shows an upturn curvature (fig.11) near Tc which can be also explained by a competition between desorder effects and superconductivity and fits a law :
$Hc_2 \sim (T_J - T)^p$ p = 1.26 in accordance with the Imry et Al scaling theory[16]. Such localisation effects will be described in more details elsewhere[17].

$Hc_{//}$ follows a $(T - Tc)^{1/2}$ law near Tc indicating film thickness limitations when ξ (T) reach the film thickness. For lower temperature, the critical fields reached values near that of sample B with $(H//(o) \simeq 290$ kOe) indicating that the intragrain resistivity limits the critical fields data in the low tempera- ture range where the coherence length is short comparative to the grain size $2\xi(T) \simeq D_G$.

Sample B follows approximately the Werthamer et Al theory[18] as observed by Askin et Al[19] with a large anisotropy $H\perp(T)/H_{//}(T) \simeq 1.5$ in the whole temperature range. Such a behavior may be related to the columnar growth observed in the film and the inhomogeneity across the film chickness. Using the GLAG equation :
$Hc_2(0) = 3.1 \times 10^4 \gamma_n \rho_o Tc$ with $Hc_2(0) = 300$ KOe and $Tc = 16.43$ K, γ_n electronic specific heat $= 3.2.10^3$ erg cm-1 K^{-2} one finds $\rho_o = 190 \mu\Omega cm$, and $\xi(0)$ is about 3.2 nm consistant with our data.

Penetration depth

The large penetration depth often observed in high resistivity NbN films results in large kinetic inductances and does not prevent diodes against flux trapping. $\lambda(T)$ and Rs (T) surface resistance were measured on NbN films deposited on Niobium end-plates of RF superconducting cavity working at about 9 GHz as described elsewhere[20].
$\lambda(T)$ is compared to the BCS relation $\lambda_{BCS}(T) = \lambda_o (1 - (T/Tc)^4)^{-1/2}$

One obtains λ_o = 375 nm for a film deposited at 20 mtorr with $\rho_{20 K} = 585 \mu\Omega cm$.
λ_o is in close agreement with Kubo et Al results[21] and with the calculated value λ_{oc} = 360 nm using the GLAG theory in the dirty limit including strong coupling factor.

$$\lambda_{oc}(nm) = 95.3 \, (\rho_o(\mu\Omega cm)/Tc(K))^{1/2}.$$

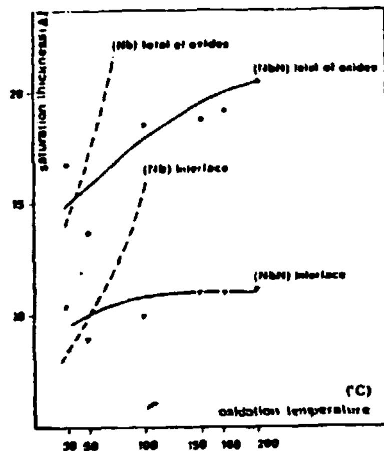

Figure 12 : XPS data on Nb and NbN oxide growth.

The maximum intragrain resistivity 250 $\mu\Omega cm$[13] is introduced for ρ_o better than the measured resistivity . he ρ(T) behavior exhibits a strong deviation from BCS theory at low temperature which can be induced by weak superconducting regions with Tc eff $\simeq$ 7.5 K. At higher temperature, the contribution of these regions which can be associated with the grain boundary presence is temperature-independent represented by λ_1 = 20 nm.

The surface resistance decreases exponentially with reduced temperature in the temperature range measurement leading to 6.5 $10^{-4} \Omega$ at T = 10 K better than previous results[22]. Further improvements will be obtained with the lower pressure deposited films where ρ 20 K = 150 $\mu\Omega cm$ is lower than the ρ_{imax}.

Critical current density

Critical current densities Jc(T) measured in 70 m wide NbN lines deposited at 20 mtorr follow a linear temperature dependence
$Jc(T) = J\delta \, (1 - T/Tc^*)$
in the temperature range
$0.5 < T/Tc < 0.95$ with $Tc - Tc^* \simeq 0.4$ K
and $Jc(0) \simeq 2 - 3.10^6$ A/cm^{-2}.

Such a variation has been analysed by Kampwith and Gray[6] in term of Josephson coupling between grains which can be applied for the resistivity range observed for the high pressure range part of the study.

Oxide growth and tunneling characteristics

XPS study of NbN oxidation

A detailed investigation of NbN and Nb film RF sputter cleaning and oxidation have been done in a especially built UHV system with analysis and oxidation chambers.

XPS is used for qu...titative analysis associated with ellipsometry and Auger investigations. The quantitative method and main results described elsewhere[23], seem to be in good accordance with others publications[24, 5]. The main observations are :

- the difficulty to remove the 1.5 nm of the stable thermal oxide formed very rapidly on the films,
- the voltage dependent damage induced by sputter etching and the field-driven rf plasma oxidation which depends on the initial surface oxide
- the stable oxide formed by thermal oxidation between 20 to 200°C is 2.0 nm thick at 200°C as shown on

Fig.12. The kinetics reaches rapidly a saturation thickness which weakly depends on pressure in the range 10^{-5} - 10^{-2} torr of pure oxygen.

- the tunnel oxide is amorphous and of the form $Nb_2(O_x N_{1-x})_{5-y}$ similar to Nb_2O_{5-y} formed on Nb films but the oxinitride composition is difficult to analyse.

A sharp interface (1.0 nm thick) formed of suboxides is found temperature independent up to 200°C.

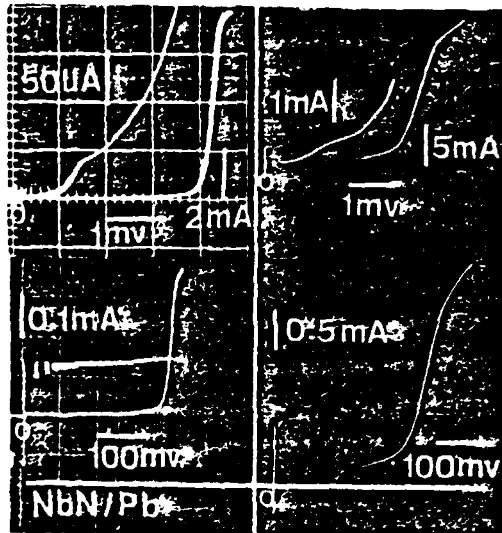

Figure 13 : I-V curves for single and 100 in-series ($10 \times 10\ \mu m^2$) diodes.

Tunneling characteristics

Typical I-V curves

As pointed out by other authors[5, 9, 10] very low subgap leakage currents ($V_m \simeq 110$ mV at 4K) are observed in NbN-oxide-Pb diodes with a thermal oxide barrier done after a light back sputter cleaning at low cathode self bias voltages ($V_{BV} \simeq 200$ Volts).

A classical lift-off resist stencil technique was used to define an array of 100 diodes $10 \times 10\ \mu m^2$ showing a critical current density of 1350 A/cm² with a spread of about ∓ 5 % mainly due to lithographic area spread (fig.13). NbN-oxide Pb edge junctions give $V_m \simeq 60$ mV with critical current $J_c \simeq 10^4$ A/cm².

NbN.NbN junctions fabricated by the SNOP or by the simple overlap method show more subgap leakage currents (table 3) corresponding to Vm values in the 8 to 16 mV range at 4K depending on the wafer processing but with a small density spread up to 10^4 A/cm². While the first electrode shows no proximity effect and the strong coupling constant is good ($2\Delta e/kTc \simeq 4.2$), the counterelectrode has typically a low gap energy measured $\Delta_{4.2} = 1.30$ meV, increasing to 1.39 meV at 1.78 K which corresponds to a reduced $2\Delta e/k_B Tc$ ($\simeq 2$) where Tc is the bulk film value.

Table 2 : Tunneling data in NbN junctions

NbN_I/NbN_{II}		Δ_I meV	Tc_I	Δ_{II}	Tc_{II}	J(A/cm²)	Vm(meV)
A	4.2 K	2.75	15.5	1.30	16.2	9.5 10^3	16
B	4.3 K	2.35	14.2	1.30	16.8	2.2 10^3	12
	1.8 K	2.40	14.2	1.39	16.8	2.2 10^3	14
NbN/Pb							
	4.2 K	2.90	16.2	1.20	7.1	1.5 10^3	115

An approximate $Tc^* = 8$ K is found for the reduced effective critical temperature induced in the oxide-NbN_{II} interface layer which is close to the T^*_c value characteristic of the weak superconducting grain boundary regions inducing excess penetration depth.

Different models can account for such a behavior but a close relation is found between the grain boundary size associated to the 6 nm diameter grain size near the interface $D_G = 2\xi(0)$ and the Tc and gap values measured (ref. fig.5).

The temperature dependence of the tunnel conductance G(T) near V = 0 volt follows the Simmons theory[25] of thermally activated tunneling being :

$$G(T)/G(0) = 1 + (a^2/\bar{\varnothing})T^2$$

in the 0-100 K range.

However, tunnel activation is found to be approximately 8 times higher for NbN/NbN diodes comparatively to NbN/Pb diodes for a similar current density indicating that mean tunnel barrier is lower for All-NbN diodes. Extra tunneling channels associated with excess current increase are probably formed by NbN counterelectrode reaction with the tunnel oxide.

Measurements in a NbN-oxide-Pb diode with low excess current lead to approximately $\bar{\varnothing} \simeq 0.3$ e V close to the potential barrier observed in Nb/Pb diodes[26] and consistent with the oxide capacitance level of about 10 µF.cm^{-2} ($J_c \simeq 10^3$ A/cm²) that we observed by Fisk internal resonances.

Summary and conclusion

High Tc (≥ 16.4 K) and positive resistivity ratios are obtained in NbN counterelectrode films without substrate heating if optimum deposition rates, gas pressure and Nitrogen/Argon flows are set. However, the Tc and gap energy are found to be grain size limited near the Oxide-NbN_{II} interface. In the coherence length scale (~ 5 nm) grains ($D_G \simeq 6$ nm) are surrounded by excess Nitrogen and voids which leads to a competition between superconductivity and desorder effects. According to the scaling theory of localisation, the metallic or insulating behavior of the system is determined by the conductance of a simple grain $G_G = E_T/\Delta E$, E_T being the characteristic tunneling energy through the insulating barrier formed by the grain boundary of size D_B :

$E_T \sim \exp(-\varnothing_B . D_B)$ and ΔE the energy separation between the energy levels of a single grain $\Delta E \sim D_G^{-3}$.

To obtain stable superconductive and resistive properties G_G must be increased far from the critical value Gc of localisation .

As $G_G \sim D_G^3 \exp(-\varnothing_B D_B)$ such a result can be obtained by decreasing $\varnothing_B$, D_B or by increasing D_G near the interface.

The attempt to increase D_G by heating up to 200°C for counterelectrode deposition leads to some increase of Δ_2 (counterelectrode gap energy) but also to excess current increase induced by NbN_{II} reacting with tunnel barrier. So the counter electrode must be deposited at low temperature. As shown on fig.6, low pressure deposition ($P_T \simeq 10$ mtorr) leads to a decrease of the resistivity and to a relative increase of Tc compared to higher pressure data. Grain boundary size is negligeable, local defects and impurities are the major effect reducing the Tc in this range. A carefull study of the damage effect, defect annealing, radiation damage induced by sputtering with different gas Argon, Krypton, Neon can lead to optimize in the future, the initial counterelectrode deposition in view to obtain a sharp and high gap energy interface.

Post-treatments

The post-processing of the electrodes allows to do

post-treatments after the trilayer deposition. NbN junctions could be baked up to 300°C without tunnel barrier change and with a controlable J_c increase between 300-400°C. Other post-treatments can be done : ion implantation, grain boundary diffusion, selective plasma treatment to modify the interface condition. Such treatments can be controlled by the tunnel conductance measurements at room temperature.

NbN junctions but also other B1-Carbides or Nitrides (MoN, TaN...) and possibly A15 diodes would be reliable and of high quality in the near future.

Acknowledgments

The authors would like to thank B. Desloges, E. Fontanet, M. Levis, V. Muffato for their technical assistance, E. Akkermans, R. Chicault, M. Dupuy, A. Ermolieff, O. Laborde, Y. Monfort, G. Rolland, T. Viet for offering us the various analysis data and their valuable collaboration.

References

1. L.N. SMITH, H. KROGER, D.W. JILLIE, IEEE Trans.Magn. MAG 19, 787, 1983
2. E.J. CUKAUSKAS, Jap.54, 1013, 1983
   E.J. CUKAUSKAS, M. NISENOFF, D.W. JILLIE, H.KROGER L.N. SMITH, IEEE, Trans.Magn., MAG 19, 831, 1983
3. M. GURVITCH, M.A. WASHINGTON, H.A. HUGGINS, J.M. ROWELL, IEEE Trans.Magn., MAG 19, 791, 1983
4. A. SOJI, S. KOSAKA, F. SHINOKI, M. AOYAGI, H. HAYAKAWA, IEEE, Trans. Magn., MAG 19, 827, 1983
   H. HAYAKAWA, Proc.LT17 Vol.III, North Holland, 1984
5. M. HIKITA, K. TAKEI, M. IGARASHI, J.Appl.Phys. 54, 7066, 1983,
   M. HIKITA, K. TAKEI, T. IWATA, M. IGARASHI, Jap. J. Appl. Phys. 21, 724, 1982
6 R.T. KAMPWITH, K.E. GRAY, IEEE Trans.Magn. MAG 17 565, 1981
7. A. AUBERT, J. SPITZ, Le Vide 175, 1, 1975
8. D.D. BACON et Al, J.Appl.Phys 54, 6509, 1983
9. V.M. PAN et Al, Cryogenics, 258, 1983
10. R.B. VAN DOVER, D.D. BACON, W.R. SINCLAIR, Appl.Phys. Lett. 41, 764, 1982
11. M. GONICHE, LETI/MEM Int.Report 84.163, 1984
12. J.C. VILLEGIER, J.C. VELER, IEEE, Trans. Magn. MAG 19, 946, 1983
13. R.R. HAKE, Appl.Phys.Lett. 10, 189, 1967
14. H.C. JONES, Appl.Phys.Lett. 27, 471, 1975
15. B.R. ZHAO, L. CHEN, H.L. LUO, M.D. JACK, D.P. MULLIN, Phys. Rev. B, 29, 6198, 1984
16. S.A. WOLF, D.V. GUBSER, Y. IMRY Phys. Rev. Lett. 42, 324, 1979
17. E. AKKERMANS, O. LABORDE, J.C. VILLEGIER to be published
18. N.R. WERTHAMER, E. HELFAND, P.C. HOHENBERG Phys.Rev. 147, 295, 1966
19. M. HASHKIN, J.R. GAVALER, J. GREGGI, M. DECROUX J. Appl.Phys. 55, 1044, 1984
20. V. NGUGEN THONG, L. WARTSKI, M. BOUSSOUKAYA, K. M'BAYE, M. PHAM TU, J.C. VILLEGIER, CERN Int. on RF Superconductivity, July, 1984
21. S. KUBO, M. ASAHI, M. HIKITA, M. IGARASHI Appl.Phys.Lett. 44, 258, 1984
22. S. ISAGAWA, J.Appl.Phys. 52, 921, 1981
23. A. ERMOLIEFF, M. GIRARD, C. RAOUL, C. BERTHAND, T. MINH DUC, Proc.6th Symp.on Appl.Surface Analysis, Dayton, June, 1984
24. R.P.FRANKENTHAL, D.J. SICONOLFI, W.R. SINCLAIR D.D. BACON, J. Electrochem.Soc.130, 2056, 1983
25. J.G. SIMMONS, J.Appl.Phys. 35, 2655, 1964
26. S.T. RUGGIERO, G.B. ARNOLD, E. TRACK, D.E. PROBER Proc. LT17, 847, North Holland, 1984
27. E. KAY, G.HEIM, J.Appl.Phys. 49, 4862, 1978.